J Solid State Electrochem (2002) 6: 468 – 474
DOI 10.1007/s10008-001-0259-y

ORIGINAL PAPER

E. Strauss · D. Golodnitsky · E. Peled

Elucidation of the charge-discharge mechanism of lithium/polymer electrolyte/pyrite batteries

Received: 30 July 2001 / Accepted: 25 October 2001 / Published online: 13 December 2001

Abstract The purpose of this work is the elucidation of the charge-discharge mechanism in the all-solid-state lithium/composite polymer electrolyte/pyrite battery operating at 120–135 °C. The main focus is the explanation of the unexpected potential jump at 1.85 V during the charge process. Effects on the charge-discharge mechanism of particle size, pyrolysis, alumina addition and Zn doping of the pyrite-based cathode are addressed. Analysis of the experimental data, as well as the structure of the charge-discharge intermediates, diffusion of lithium and iron cations in the composite cathode, suggests that the sudden charge overpotential is associated with slow mass transport of iron(II) cations through the Li_2FeS_2 phase.

Keywords Polymer electrolytes · Lithium batteries · Mechanism

Introduction

Much effort has gone into the investigation of the charge-discharge of pyrite in the high-energy-density Li/FeS_2 battery systems and several discharge mechanisms have been proposed. It was found that the discharge of FeS_2 in nonaqueous and polymer electrolytes as well as in molten media proceeds as a multi-stage process with the formation of metallic iron and lithium sulfide as the final discharge products. Extensive studies have been made of high-temperature (450 °C) cells with LiCl/KCl eutectic molten electrolytes [1, 2]. The cells showed excellent reversibility. Tomczuk et al. [2] proposed the formation during discharge of $Li_3Fe_2S_4$, $Li_{11}Fe_4S_{10}$ and Li_2FeS_2 as lithiated intermediates. For the Li/pyrite system in nonaqueous electrolyte, Nardi et al. [3] suggested the formation of Li_3FeS_4 during discharge, Iwakura et al. [4] and Ikeda et al. [5] proposed the formation of Li_2FeS_2 as the only intermediate, and Hansen and West [6] assumed that cycling Li/FeS_2 cells in $LiPF_6$/EC:DEC electrolyte at room temperature involves the iron monosulfide. Three phases have been characterized by Brec et al. [7] using Mossbauer spectroscopy at room temperature. These were Li_xFeS_2 (γ) ($1.09 \le x < 1.5$), Li_xFeS_2 (v) ($1.5 \le x < 2$) and $Li_{x\approx 0}FeS_2$ (λ). It has been demonstrated also [8] that Li_2FeS_2 is a compound that can be deintercalated at charge. The first lithium removal corresponds to the oxidation of iron. Deintercalation of the second lithium results in the oxidation of sulfur, the final structure of the completely oxidized phase being $Fe^{3+}\left(S_2^{2-}\right)_{1/2}S^{2-}$. Scherson [9] states that the most probable structure of the two-electron discharged material in the Li/Li(triflate)DME:dioxolane/FeS_2 cell involves a highly disordered, possibly amorphous, form of pyrrhotite, $Fe_{1-x}S$, with Li^+ counterbalancing the charge. All the room-temperature cells studied showed extremely poor reversibility or none at all [3, 4, 5, 6, 10].

We were the first to show the excellent reversibility of Li/composite polymer electrolyte (CPE)/FeS_2 cells at 90–135 °C [11]. Charge-discharge processes in the Li/LiI-$P(EO)_n$-Al_2O_3-based CPE/pyrite battery over a long-term cycle life have been analyzed with the use of dQ/dV curves [12]. Up to seven phases have been identified and found to change during the first 50–100 cycles. These phases do not change much over the subsequent 400 cycles. The major phases have been recently identified by EXAFS and NEXAFS measurements [13]. It was shown that reduction of the ferrous disulfide proceeds as a multi-stage process via Li_2FeS_2 to metallic iron. No evidence of FeS was found.

In this work, elucidation of the charge-discharge mechanism in Li/CPE/FeS_2 cells has been attempted. To clarify the charge-discharge processes and, in particular, to find the explanation for the unexpected potential jump at 1.85 V on charge, the electrochemical behavior of pristine, Zn-doped, and pyrolyzed pyrite was studied.

E. Strauss · D. Golodnitsky (✉) · E. Peled
School of Chemistry,
Tel Aviv University, Tel Aviv 69978, Israel
E-mail: golod@post.tau.ac.il

Experimental

The electrochemical cells studied comprise a lithium anode, a LiI-$P(EO)_{20}$-EC_1-(9% by volume, v/v) Al_2O_3 composite polymer electrolyte and a 50% v/v pyrite-based composite cathode. The electrolytes were prepared from poly(ethylene oxide) [P(EO)] (Aldrich, average molecular weight 5×10^6), which had been vacuum dried at 45–50 °C for about 24 h. The LiI (Aldrich) was vacuum dried at 200–230 °C for about 8 h. All subsequent handling of these materials took place under an argon atmosphere in a VAC glove box containing less than 10 ppm water. The detailed procedure of the polymer electrolyte preparation has been described elsewhere [11, 12, 13].

The 45-μm-thick cathode foil was prepared by dispersing natural pyrite particles (''Technicks'', Chemalloy less than 44 μm size) in a polymer slurry and cast on a Teflon tray. For the preparation of ultrathin 10 μm cathodes, fine FeS_2 powder was used. Grounding of pre-dried pyrite was performed in a hermetically sealed ball mill for 48 h. Following carefully all the steps of cathode preparation we have achieved reproducibility of battery performance (utilization of cathode active material, reversible capacity, charge-discharge overpotential) in the range of 2–5%.

The 0.95 cm^2 cells composed of a lithium anode, a 100–150 μm CPE film and a composite cathode were held under spring pressure inside the hermetically sealed glass vessel. Before each experiment, cells were equilibrated at a given temperature for at least 2 h. The batteries were cycled at 120 and 135 °C in a Maccor series 2000 battery test system.

Results and discussion

A porous composite cathode can be considered to consist of two contiguous interwoven networks [14]. The cathode-active material network consists of electronically conducting particles in contact with each other. The other network of the composite cathode is a polymer electrolyte that fills the pores between the active cathode material particles. The lithium ions participating in the cathode reaction and originating from the lithium electrode migrate through the CPE into the PE-filled pores of the composite cathode to a site in the interior of the electrode, where they react with the cathode-active material. The mobility of ions in the polymer-electrolyte phase of a composite cathode should be comparable with that in the cathode active-material phase. Thus it may have a very pronounced influence on the total ion transport in the composite cathode and the mechanism of charge-discharge may be equally affected by ion transport in the electrolyte network and by redox and insertion kinetics of the cathode-active material.

We previously found [15] that the limiting current density (i_{lim}) in LiI-$P(EO)_n$-Al_2O_3 CPEs increased monotonically from 0.3 to 2.3 mA/cm^2 with n varying from 80 to 9. The ion pairs are formed in concentrated CPEs ($n \le 20$), which reduce the effective concentration of charge carriers and contribute an additional term to the diffusion impedance. On the basis of these experimental data, the LiI-$P(EO)_{20}$-Al_2O_3 composite polymer electrolyte, characterized by high conductivity (3–5 mS/cm at 120 °C) and a high diffusion coefficient of lithium (1.6×10^{-7} cm^2/s [15]), was chosen as the electrolyte in the Li/CPE/FeS_2 battery. Taking into account that the operating charge and discharge current density in the Li/CPE/pyrite battery is much lower than i_{lim}, and assuming that D_{Li+} in the CPE should be comparable to that in the pores of cathode, filled by the same electrolyte, we believe that lithium mass transport in the solid cathode does not impede the overall charge-discharge process of the Li/CPE/pyrite battery.

For a Li/CPE/FeS_2 cell, the first discharge curve at 90–135 °C has two plateaus, one at about 1.8 V and another at 1.6 V. Figure 1 shows the first discharge represented as V versus capacity (a) and V versus dQ/dV (b) curves. The prolonged plateaus seen in curve (a) appear in the V versus dQ/dV (b) curves as sharp peaks. Thorough dQ/dV analysis of high-resolution voltage measurements allows detailed consideration of the fine changes occurring on charge-discharge. The reduction of FeS_2 in the first cycle occurs in two steps (reactions 1 and 2):

$$FeS_2 + 2Li^+ + 2e^- \rightarrow Li_2FeS_2 \quad (1)$$

$$Li_2FeS_2 + 2Li^+ + 2e^- \rightarrow Fe + 2Li_2S \quad (2)$$

It has been found [16] that the particle size of the discharge products of the Li/$LiClO_4$-PC/FeS_2 cell depends on the rate of discharge. At 325 $\mu A/cm^2$, 3.6-nm-diameter iron supermagnetic crystallites are formed. As was verified by chemical and XRD analysis [17], 7-nm-particle size lithium sulfide was found at the end of discharge when 40-μm-size pyrite was used. This indicates a loosening of the electrode structure (Fig. 2). The change in the solids volume, calculated from the crystallographic molar volume of the compounds involved in the reaction, shows a dramatic increase of about 250% ($V_{m(FeS_2)}$ = 24.5 mL/mol, $V_{m(Fe)}$ = 8.0 mL/mol, $V_{m(Li_2S)}$ = 27.7 mL/mol) at the end of the first discharge. Creeping of both the cathode and CPE can be prevented by the addition of alumina and increasing the spring pressure.

Over the operating temperature range of 120–135 °C, pyrite is not regenerated on charge; therefore the discharge curves from the second cycle onwards differ from the first cycle [11, 12, 13, 18] (Fig. 3). The simplified charge-discharge mechanism of pyrite in polymer electrolytes has been studied extensively [12, 13] and may be schematically described by the following reactions:

$$Fe + 2Li_2S - 2e^- \rightarrow Li_2FeS_2 + 2Li^+ \quad (3)$$

$$Li_2FeS_2 - xLi^+ - xe^- \rightarrow Li_{2-x}FeS_2 (0.5 < x < 0.8) \quad (4)$$

It has been suggested [19] that in the Li/CPE/FeS_2 cell at 135 °C a charge-protection shuttle mechanism is described by reactions 5 and 6:

$$\begin{aligned} Li_{2-x}FeS_2 - (2+\delta)e^- &\rightarrow Fe_\delta S + nS + (2-x)Li^+ \\ &\rightarrow Fe_\delta S + Li_2S_n (n > 4) \end{aligned} \quad (5)$$

$$2Li^0 + Li_2S_n \rightarrow 2Li_2S_{n/2} \quad (6)$$

At the end of the second and all subsequent discharges, the fractional change in the cathode-active-material volume is about +27%. On charge, the

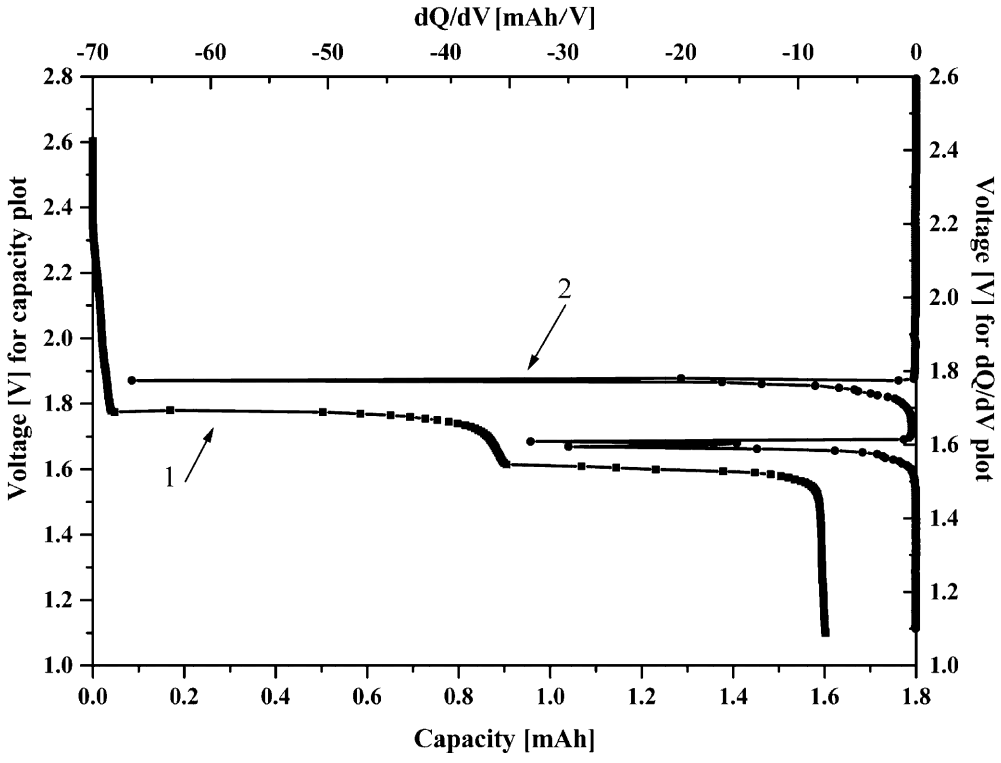

Fig. 1 First discharge of the Li/CPE/FeS_2 cell. CPE composition: LiI_1-$P(EO)_{20}$-EC_1-9% Al_2O_3. Operation conditions: $T = 135$ °C, i.d. = 0.05 mA/cm^2; cathode composition: 50% (v/v) FeS_2, 50% (v/v) CPE; cathode thickness: 10 μm. *Curve 1*: voltage versus capacity curve; *curve 2*: voltage versus dQ/dV

cathode contracts by about 21%. As the operating temperature is 120–135 °C, we believe that, on charge, completely molten polymer electrolyte fills the pores, thus preventing the separation of cathode-active-material particles and providing ion conduction between them.

With the help of Eqs. 3, 4, 5, the overall charge-discharge curves (Fig. 3a) may be divided into three main voltage regions, and dQ/dV curves of high-resolution voltage measurements, presented in the same figure, permit a detailed analysis of the reactions taking place. Regions B and C are associated with reversible electrochemical reaction 3. Regions A and D are attributed to the reversible insertion/deinsertion of lithium in the Li_2FeS_2 host, complicated by a phase change [7]. Region E is attributed to the formation of pyrrhotite and lithium polysulfides (reaction 5).

The discharge capacity over the high-voltage range (part A of the curve) showed very high stability. The capacity loss of the 1.6–2.2 V region over the first 100 cycles was only 0.22%/cycle, while that of the 1.1–1.6 V region was 0.45%/cycle (Fig. 4). This indicates that the insertion-deinsertion step of the discharge process is highly reversible. However, on long-time cycling, the capacity loss of the two-electron reaction branch of the curve approaches that of the intercalation-deintercalation region. We believe that this may be related to the formation of the additional phase at 1.3 V, caused presumably by the interaction of small particles of iron with the electrolyte. The charge-discharge of this phase proceeds from 1.4 to 1.8 V, thus not contributing to the intercalation capacity.

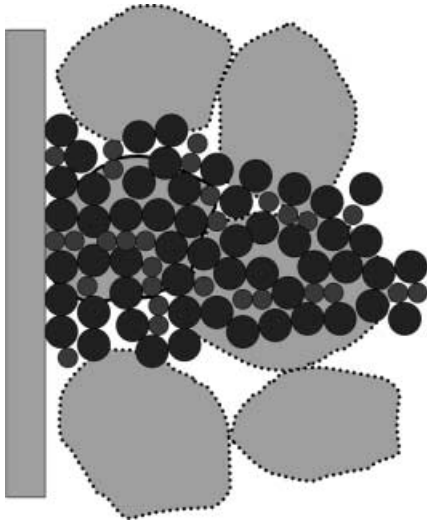

Fig. 2 Schematic presentation of the loosening of cathode active-material structure at the end of the first discharge. *Medium circles*: Li_2S; *small circles*: Fe^0; *large irregular-shape particles*: pyrite

According to Eq. 3, and on the basis of our previous data on the long cycle life of the Li/CPE/FeS_2 cell, the two-electron transition on charge-discharge should be completely reversible, the charge curve should follow the dashed (Fig. 3a) line and the reaction should proceed at the same Li/Fe ratio. However, as can be seen from Fig. 3a, the experimental charge curve shows significant deviation from that expected and a sudden voltage jump occurs at a lower Li/Fe ratio as compared with discharge.

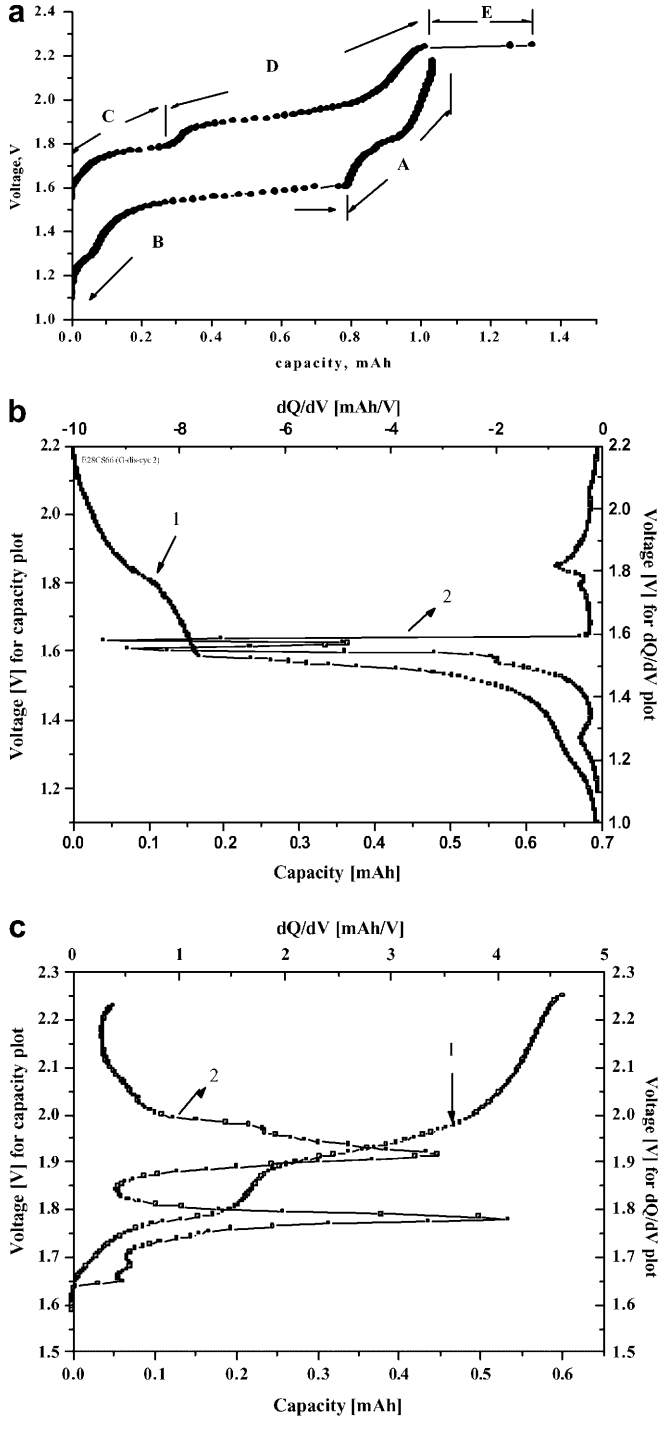

Fig. 3 **a** Typical charge-discharge curves of Li/CPE/FeS_2 cell (cycle 2). *A*, *B*, *C*, and *D*: the main voltage regions (detailed explanation in text). **b** Discharge curve of Li/CPE/FeS_2 cell (cycle 2). *Curve 1*: voltage versus capacity curve; *curve 2*: voltage versus dQ/dV. **c** Charge curve of Li/CPE/FeS_2 cell (cycle 2). *Curve 1*: voltage versus capacity curve; *curve 2*: voltage versus dQ/dV

Several factors affect this phenomenon. The relative prolongation of charge regions C and D (represented as a normalized capacity) is strongly affected by the size of the pyrite particles. An almost two-fold increase in the normalized capacity of the charge region C (from 30–37 to 60%) was observed when cycling thin cathodes composed of less than 5 μm FeS_2 particles as compared to those of less than 10 μm pyrite (Fig. 5a). A similar capacity change was found for thick (less than 44 μm) versus thin (less than 10 μm particle size) FeS_2 cathodes (Fig. 5b). We assume that these changes are due to the increased surface area of the cathode-active material participating in the reduction process. Addition of 15-nm alumina to the composite cathode results in a shift of the 1.85 V charge voltage jump towards higher capacity values of region C. Its normalized capacity increased from 30 to 66% in the cathodes without alumina and in those containing 15% (v/v) Al_2O_3. We believe that the high-surface-area nanosize alumina eliminates the sticking of cathode-active material particles and subsequent formation of large aggregates.

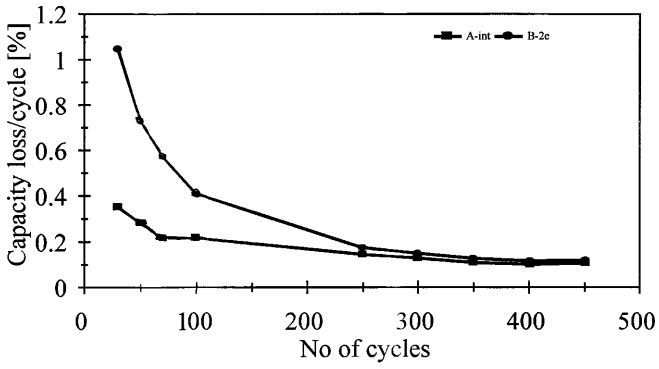

Fig. 4 Plot of discharge capacity loss versus number of cycles for region A and region B (see Fig. 3). Capacity losses are calculated individually with respect to high- and low-voltage regions

In order to favour lithium and iron solid-state migration in the composite cathode, we attempted to create additional sulfur vacancies in the cathode-active material network by sulfur release. As expected, pyrolysis of the pyrite at 450 °C caused up to a 100 mV decrease in the charge overvoltage (Fig. 6).

Doping of pyrite with a foreign cation, such as Zn, followed by pyrolysis was expected to further improve the ion transport. However, reversible utilization of the 45-μm-thick cathode composed of Zn-doped pyrite that had undergone pyrolysis decreased from 70 to 30%. The charge overpotential of region D was found to be unexpectedly high and the corresponding capacity decreased. XPS analysis showed the formation of zinc sulfide (as a result of FeS_2-Zn pyrolysis) that can participate in the charge-discharge of the Li/CPE/FeS_2-ZnS cell. The reaction occurs at 1.6 V, with the possible formation of Li_2ZnS_2 or $Li_2Fe_{2-x}Zn_xS_2$. The radius of Zn^{2+} is smaller than that of Fe^{2+}; therefore it can compete with the migration of the iron cation and impede the Fe^{2+} transport in the $Li_2Fe_{2-x}Zn_xS_2$ as compared to the Li_2FeS_2. This may explain the charge problems found in the Li/CPE/FeS_2 + ZnS battery.

Some idea of the sudden voltage jump occurring on charge of the Li/CPE/FeS_2 battery can be gained from the schematic presentation of the all-solid-state pyrite-based composite cathode in Fig. 7. We assume that the

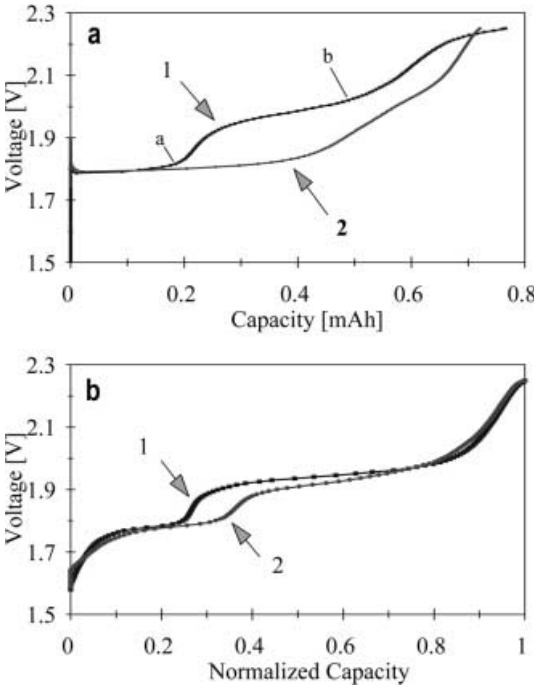

Fig. 5 **a** Charge curves of Li/CPE/FeS_2 cell (cycle 2); cathodic SEI formation was performed at the first discharge, i.d. = 50 μA/cm^2, $V_{cut\text{-}off}$ = 0.1. *Curve 1*: 10-μm pyrite particles; *curve 2*: < 5-μm pyrite particles. **b** Charge curves of Li/CPE/FeS_2 cell (cycle 2). *Curve 1*: 44-μm pyrite particles; *curve 2*: 10-μm pyrite particles

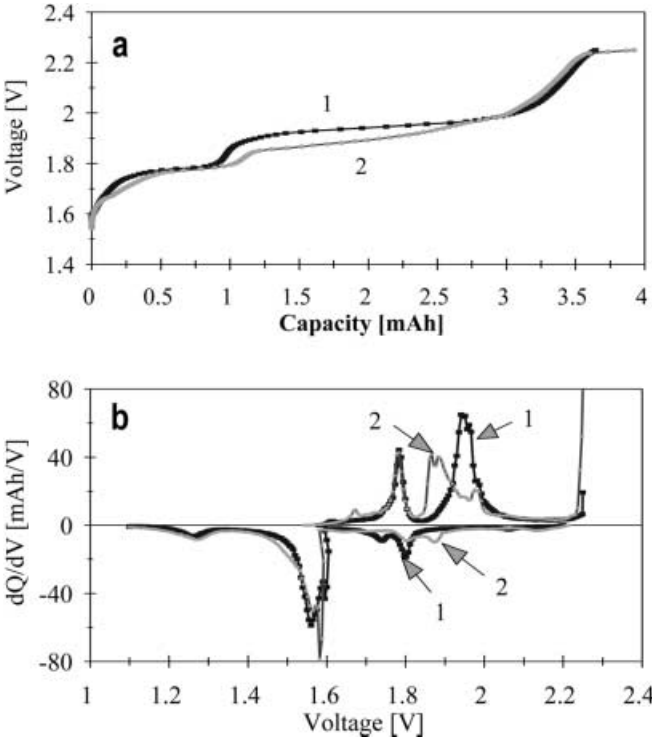

Fig. 6 **a** Charge curves of Li/CPE/FeS_2 cell (cycle 2). Cathode composition: 50% (v/v) FeS_2, 50% (v/v) CPE; cathode thickness 10 μm. CPE composition: LiI_1-$P(EO)_{20}$-EC_1-9% Al_2O_3. Operation conditions: T = 135 °C, i.d. = 0.3 mA/cm^2, i.c. = 0.05 mA/cm^2. *Curve 1*: pristine pyrite; *curve 2*: pyrite after pyrolysis. **b** dQ/dV curves of Li/CPE/FeS_2 cells at cycle 2. *Curve 1*: pristine pyrite; *curve 2*: pyrite after pyrolysis

charge mechanism (reactions 3 and 4) proceeds as follows:

1. Iron is oxidized to give Fe^{2+} at the Fe/Li_2S interface (referred to hereafter as interface α). The Fe^{2+} reacts with Li_2S, which releases two Li^+ ions, to form a Li_2FeS_2 layer in interface α (reactions 7 and 8):

$$Fe_\alpha - 2e^- \rightarrow Fe_\alpha^{2+} \quad (7)$$

$$Fe_\alpha^{2+} + 2Li_2S_\alpha - 2Li^+ \rightarrow (Li_2FeS_2)_\alpha \quad (8)$$

2. Formation of the Li_2FeS_2 layer generates two new interfaces: Fe/Li_2FeS_2 (β) and Li_2FeS_2/Li_2S (γ). In order for reaction 3 to continue, the Fe^{2+} cations that were formed at interface β move (migrate and diffuse) through lattice defects in the Li_2FeS_2 until they reach interface γ, were they meet the Li_2S (reactions 9, 10, 11):

$$Fe_\beta - 2e^- \rightarrow Fe_\beta^{2+} \quad (9)$$

$$Fe_\beta^{2+} \rightarrow Fe_\gamma^{2+} \quad (10)$$

$$Fe_\gamma^{2+} + 2Li_2S_\gamma - 2Li^+ \rightarrow (Li_2FeS_2)_\gamma \quad (11)$$

3. Step 2 continues until all the iron particles electrically connected to the current collector react with lithium sulfide particles: this leads to a thickening of the Li_2FeS_2 layer. When the layer thickness reaches a critical value, a potential jump appears at about 1.85 V (Fig. 3a). This potential jump from about 1.70 to 1.85 V (the midpoint of the voltage step) may be due to the transport limitations of Fe^{2+} in Li_2FeS_2 followed by the occurrence of an ion transport barrier similar to that of the limiting current phenomenon.

According to Blandeau et al. [20], Li_2FeS_2 can be considered as made up of FeS_2 (2D) slabs, the three-dimensionality of the phase being restored by the lithium that fills the octahedral inter-slab sites and some of its tetrahedral voids. The general formulation of the compound can be written as Li^+_{Oh} Li^+_{Td}-$Fe^{2+}_{Td}S^{2-}_2$. The Fe-S interatomic distance for the main (FeS_4) tetrahedra is 2.357 Å. For the surrounding octahedron the Fe-S distance is 2.53 Å. Li-S distances are 2.44 and 2.77 Å for the surrounding tetrahedral and octahedral lithium, respectively, indicating that iron ions are more closely packed in the layered framework of Li_2FeS_2 than are lithium ions.

A short relaxation time constant associated with a high diffusion coefficient of lithium in Li_2FeS_2 has been reported [21], thus suggesting fast lithium ion transport. Taking into account fast lithium ion transport in the polymer electrolyte network and in the Li_2FeS_2 of the composite cathode, we suggest that it is the mass transport of iron cations through the Li_2FeS_2 that slows the reaction rate of Eq. 3 and creates a charge overvoltage. The generated

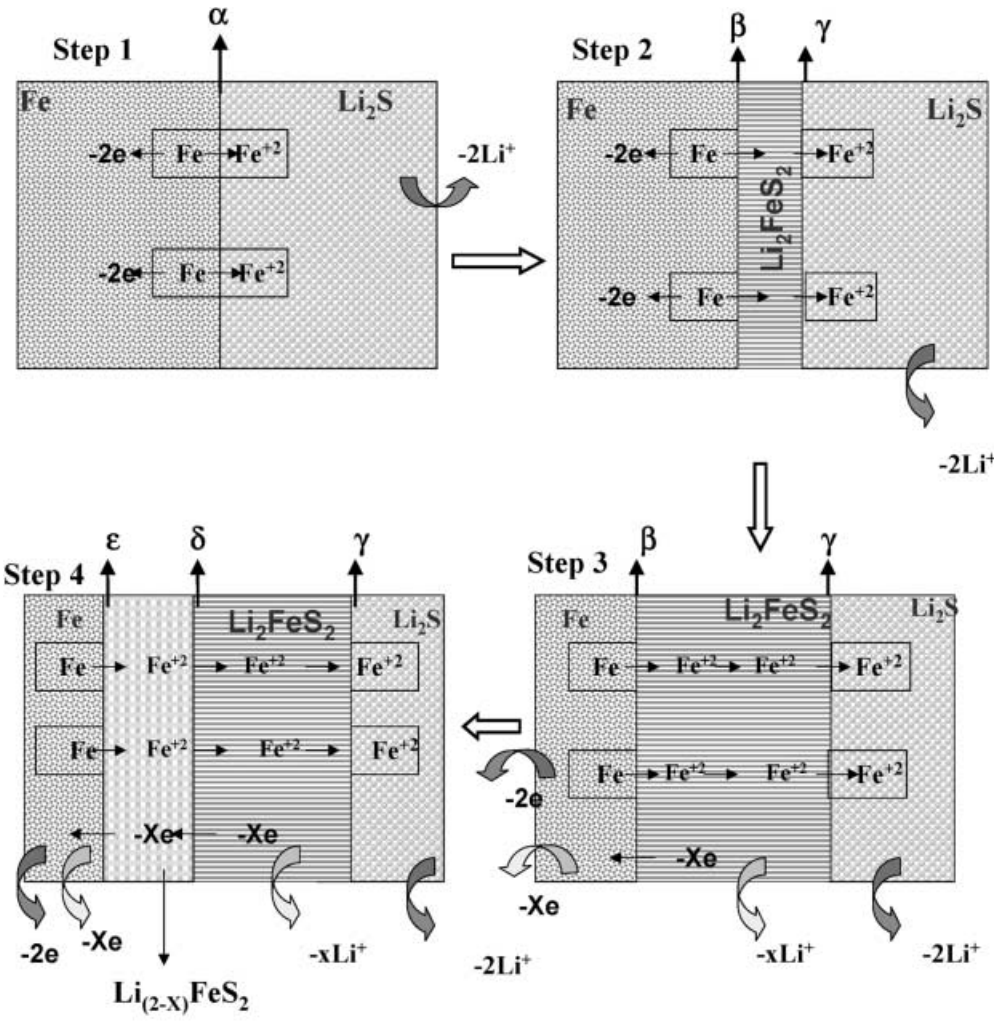

Fig. 7 Schematic representation of the charge solid-phase transitions in a pyrite-based composite cathode

overpotential may be high enough to enable the initiation of the deintercalation process (Eq. 4).

4. The new phase, $Li_{2-x}FeS_2$, may form two new interfaces, δ ($Li_2FeS_2/Li_{2-x}FeS_2$) and ε ($Li_{2-x}FeS_2/Fe$). Reactions 3 and 4 are assumed to proceed simultaneously in three different microphases (reactions 12, 13, 14, 15, 16 below).

a) β and γ interfaces (step 3 in Fig. 7): iron is oxidized to give Fe^{2+} which migrates through vacancies in $Li_{2-x}FeS_2$ and in Li_2FeS_2 until it reaches interface γ, where Fe^{2+} reacts with Li_2S to give Li_2FeS_2.

b) δ interface (step 4 in Fig. 7): Fe^{2+} is further oxidized to give Fe^{3+} in the $Li_{2-x}FeS_2$ [20, 21]:

$$Fe_{\varepsilon} - 2e^{-} \rightarrow Fe^{2+}_{\varepsilon} \quad (12)$$

$$Fe^{2+}_{\varepsilon} \rightarrow Fe^{2+}_{Li_{2-x}FeS_2} \quad (13)$$

$$Fe^{2+}_{Li_{2-x}FeS_2} \rightarrow Fe^{2+}_{Li_2FeS_2} \quad (14)$$

$$Fe^{2+}_{Li_2FeS_2} \rightarrow Fe^{2+}_{\gamma} \quad (15)$$

$$Fe^{2+}_{\gamma} + 2Li_2S_{\gamma} - 2Li^{+} \rightarrow (Li_2FeS_2)_{\gamma} \quad (16)$$

Deinsertion of lithium results in the oxidation of iron(II) to iron(III), the redox process being accompanied by a change in iron ion occupancy at an advanced stage of the reaction [20]. The electronic structure of the partially deintercalated compound can be written as $Li^{+}_{Oh}Li^{+}_{(1-x)Td}Fe^{2+}_{Td}Fe^{3+}_{Td}S_2^{2-}$, leaving a partially empty lithium tetrahedral site that may be occupied by iron ions. The compound formed is presumably characterized by the increased mobility of iron that favors reaction 4.

As shown by the Mössbauer study, some of the iron ions around $Li_{1.5}FeS_2$ shift to octahedral coordination and this transition is related to the peak on the dQ/dV curve at about 1.95 V (Fig. 3c). All the lithium cations in the $Li_{1.5}FeS_2$ were found at octahedral sites [20]. The electronic structure of the final charge product of the

lithium/composite polymer electrolyte/pyrite battery is hence $Li^{+}_{1.5Oh}Fe^{2+}_{Td}Fe^{3+}_{(1-x)Td}Fe^{3+}_{(x)Oh}S_2^{2-}$.

The positive effect of the pyrolysis of the pristine pyrite, followed by the creation of new tetrahedral vacancies that results in about 100 mV decrease in the charge overvoltage of the Li/CPE/FeS_2 cell, supports our suggestion of slow transport of Fe^{2+} in the Li_2FeS_2 phase.

Summary

To explain the sudden voltage jump occurring on charge at 1.85 V in the Li/CPE/FeS_2 cell that decreases the charge capacity of the low-voltage branch of the curve (Fig. 3a, region C), we studied the effect of particle size, pyrolysis and doping of pyrite on the charge-discharge mechanism.

An almost two-fold increase of the normalized capacity of the 1.6–1.85 V charge region was observed on cycling of thin pyrite cathodes composed of less than 5-μm-size particles as compared to those of 10-μm size. A similar charge capacity increase was achieved by the addition of 15% alumina to the cathode. Pyrolysis of the pristine pyrite performed at 450 °C caused up to a 100 mV decrease in the charge overvoltage. Pyrolysis of pyrite doped by metallic zinc caused the reversible utilization of the 45-μm-thick cathode to decrease from 70 to 30%.

Analysis of these experimental data, as well as the structure of the charge-discharge intermediates and diffusion of lithium and iron cations in the composite cathode, suggests that it is the mass transport of iron cations through the Li_2FeS_2 that slows the reaction rate (Eq. 3) and creates a charge overvoltage.

Acknowledgements We would like to thank Prof. I. Reiss (Technion, Haifa, Israel) for help in discussion of the experimental results.

References

1. Henriksen GL (1995) Lithium/iron sulfide batteries. In: Linden D (ed) Handbook of batteries. McGraw-Hill, New York, pp 39.1–39.17
2. Tomczuk Z, Tani B, Otto NC, Roche MF, Vissers DR (1982) J Electrochem Soc 129:926
3. Nardi JC, Clark MB, Evans WP (1981) Symposium on electric power sources in horological and microtechnical protection, Mulhouse, France, extended abstracts, p 48
4. Iwakura C, Isobe N, Tamura H (1983) Electrochim Acta 277:126
5. Ikeda H, Narukawa S, Nakaido S (1980) 21st battery symposium, Okayama, Japan, extended abstracts, p 47
6. Hansen K, West K (1997) Electrochem Soc Proc 97-18:124
7. Brec R, Prouzet E, Ouvrard G (1989) J Power Sources 26:325
8. Gard P, Sourisseau C, Ouvrard G, Brec R (1986) Solid State Ionics 20:231
9. Scherson DA (1996) Interface (Fall):34
10. Fong R, Dahn JR, Jones CHW (1989) J Electrochem Soc 136:3206
11. Peled E, Golodnitsky D, Ardel G, Lang J, Lavi Y (1995) J Power Sources 54:496
12. Strauss E, Golodnitsky D, Peled E (2000) Electrochim Acta 45:1519
13. Strauss E, Golodnitsky D, Peled E, Kostov S, Garan D, den Boer M, Greenbaum S (1999) J Power Sources 81–82:715
14. Atlung S, West K (1989) J Power Sources 26:139
15. Strauss E, Golodnitsky D, Ardel G, Peled E (1998) Electrochim Acta 43:1315
16. Jones CHW, Kovacs PE, Sharma RD, McMillan RS (1990) J Phys Chem 94:832
17. Strizhko AS, Govalev SN, Aksenov OV, Naumenko AF, Rayhelson LB, Shembel EM (1992) Abstracts of the 6th international meeting on lithium batteries, Munster, Germany, V-05, p 487
18. Peled E, Golodnitsky D, Penciner J (1998) Anode/electrolyte interface. In: Besenhard JO (ed) Handbook of battery materials. VCH, Weinheim, pp 410–457
19. Peled E, Golodnitsky D, Strauss E, Lang J, Lavi Y (1998) Electrochim Acta 43:1593
20. Blandeau L, Ouvrard G, Calage Y, Brec R, Rouxel J (1987) J Phys C 20:4271
21. Brec R, Dugast A (1980) Mater Res Bull 15:619